Supporting Information

A single colorimetric sensor for multiple targets: the sequential detection of Co^{2+} and cyanide and the selective detection of Cu^{2+} in aqueous solution

Hyo Jung Jang, Tae Geun Jo, Cheal Kim*

Department of Fine Chemistry and Department of Interdisciplinary Bio IT Materials, Seoul National University of Science and Technology, Seoul 139-743, Korea. Fax: +82-2-973-9149; Tel: +82-2-970-6693; E-mail: chealkim@seoultech.ac.kr

Table S1. Examples for the simultaneous detection of Co^{2+} and Cu^{2+} by organic chemosensors.

Sensor	Detection limit (μM)	Binding constant	Water % in solvent	Method of detection	Reference
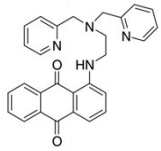	**Co^{2+}** 30 **Cu^{2+}** 30	No data	20%	Naked eye	[1]
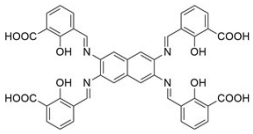	**Co^{2+}** 0.52 **Cu^{2+}** 0.41	No data	100%	Naked eye	[2]
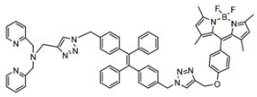	**Co^{2+}** 0.1 **Cu^{2+}** 0.1	No data	40%	Fluorescence	[3]
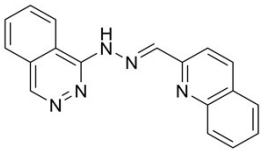	**Co^{2+}** 1.7 **Cu^{2+}** 2.1	**Co^{2+}** $1.0x10^{10}$ **Cu^{2+}** $1.0x10^{9}$	100%	Naked eye	[4]
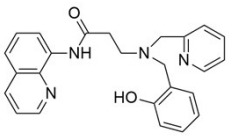	**Co^{2+}** 0.85 **Cu^{2+}** 0.98	**Co^{2+}** $1.1x10^{4}$ **Cu^{2+}** $9.9x10^{3}$	80%	Naked eye	[5]
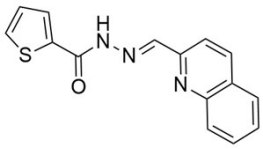	**Co^{2+}** 0.19 **Cu^{2+}** 0.13	**Co^{2+}** $1.0x10^{10}$ **Cu^{2+}** $7.0x10^{9}$	95%	Naked eye	this work

References

1 N. Kaur and S. Kumar, *Tetrahedron Lett*., 2008, **49,** 5067–5069.

2 M. R. Awual, T. Yaita and Y. Okamoto, *Sens. Actuators, B*, 2014, **203,** 71–80.

3 J. H. Ye, L. J. Duan and L. L. Jin, *Adv. Mater. Res*., 2012, **554**, 2045–2048.

4 J. J. Lee, Y. W. Choi, G. R. You, S. Y. Lee and C. Kim, *Dalton Trans*., 2015, **44**, 13305–13314.

5 E. J. Song, G. J. Park, J. J. Lee, S. Lee, I. Noh, Y. Kim, S. J. Kim, C. Kim and R. G. Harrison, *Sens. Actuators, B*, 2015, **213**, 268–275.

Table S2. Examples for the sequential detection of Co^{2+} and CN^{-} by organic chemosensors.

Sensor	Detection limit (μM)	Binding constant	Interference	Water % in solvent	Method of detection	Reference
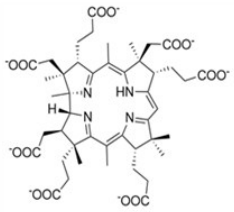	10	1.2×10^{5}	No data	100%	Naked eye	[1]
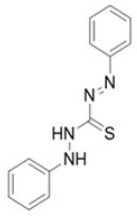	0.43	1.26×10^{7}	No interference	25%	Naked eye	[2]
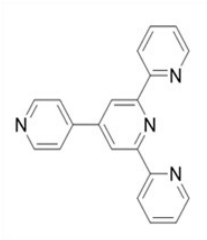	10	No data	No data	100%	Naked eye	[3]
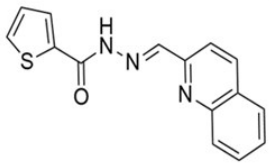	24.11	3.0×10^{4}	No interference	95%	Naked eye	this work

References

1 C. Männel-Croisé and F. Zelder, *Inorg. Chem.*, 2009, **48**, 1272–1274.

2 H. Tavallali, G. Deilamy-Rad, A. Parhami and S.Z. Mousavi, *Photochem. Photobiol. B Biol.*, 2013, **125**, 121–130.

3 I. Bhowmick, D. J. Boston, R. F. Higgins, C. M. Klug, M. P. Shores and T. Gupta, *Sens. Actuators, B*, 2016, **235**, 325–329.

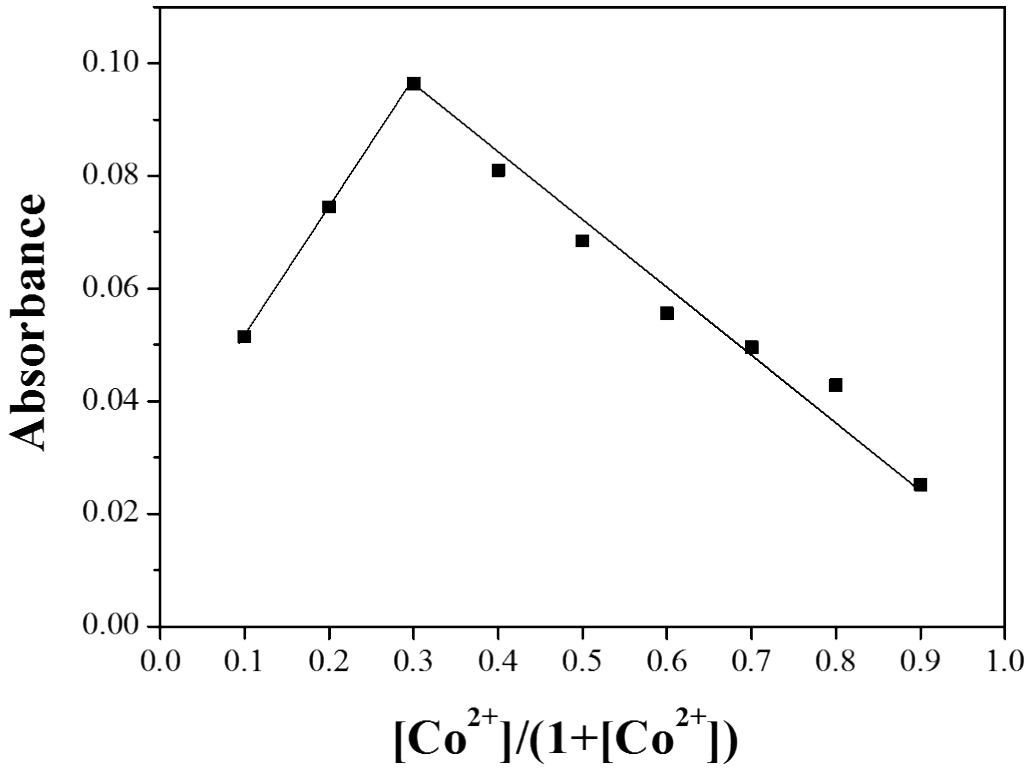

Fig. S1 Job plot for the binding of **1** with Co^{2+}. Absorbance at 400 nm was plotted as a function of the molar ratio of $[Co^{2+}]/([\mathbf{1}]+[Co^{2+}])$. The total concentration of Co^{2+} ions with sensor **1** was 2.0 x 10^{-5} M.

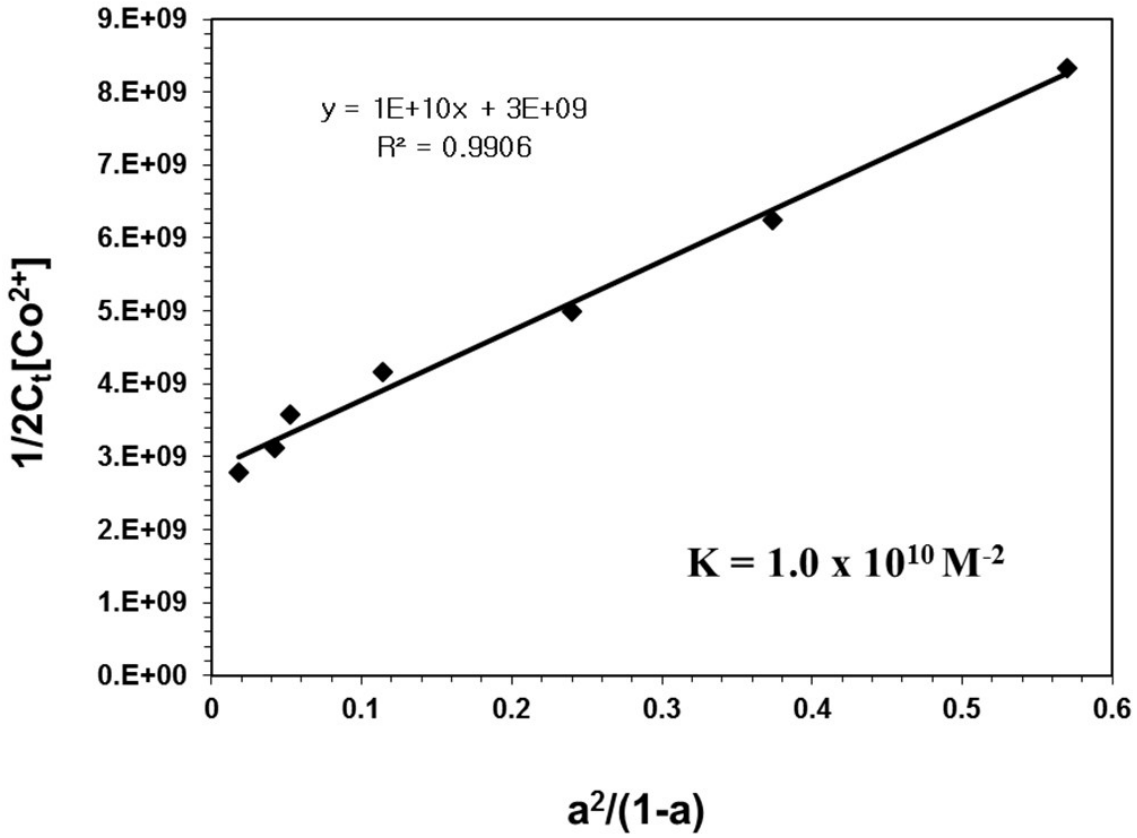

Fig. S2 Li's equation plot (absorbance at 400 nm) of **1**, assuming 2:1 stoichiometry for association between **1** and Co^{2+}. 'Ct' means the concentration of **1**, and 'a' does $[(A_x-A_{max})/(A_0-A_{max})]$.

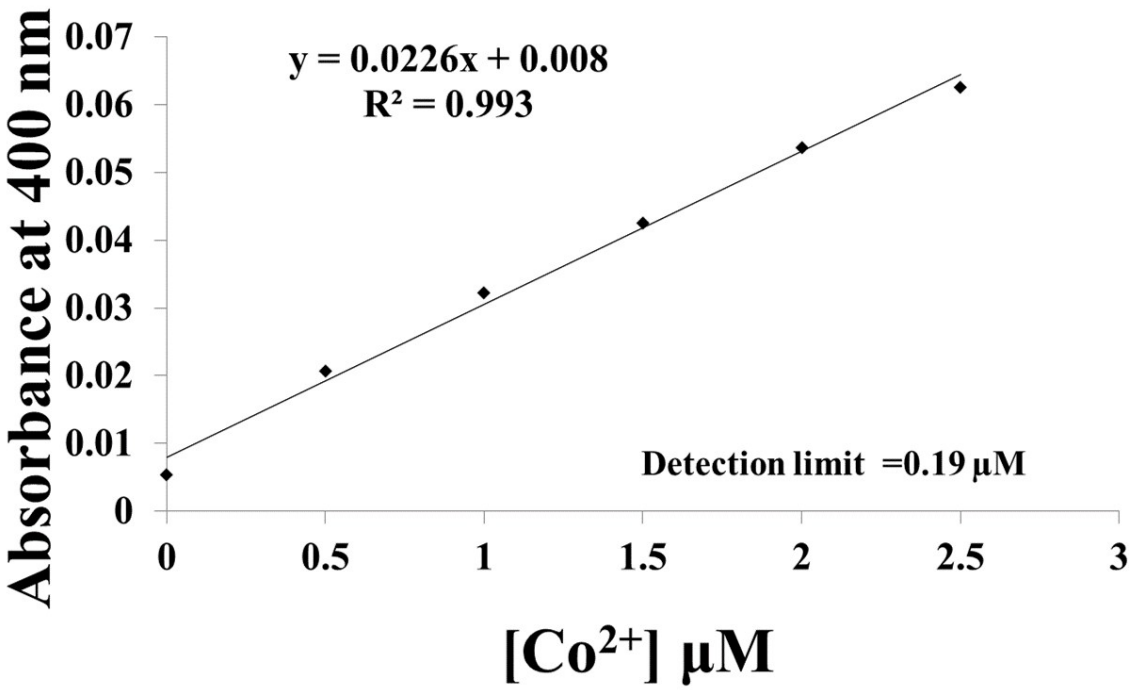

Fig. S3 Detection limit based on change in the ratio (absorbance at 400 nm) of **1** (20 μM) with Co^{2+}.

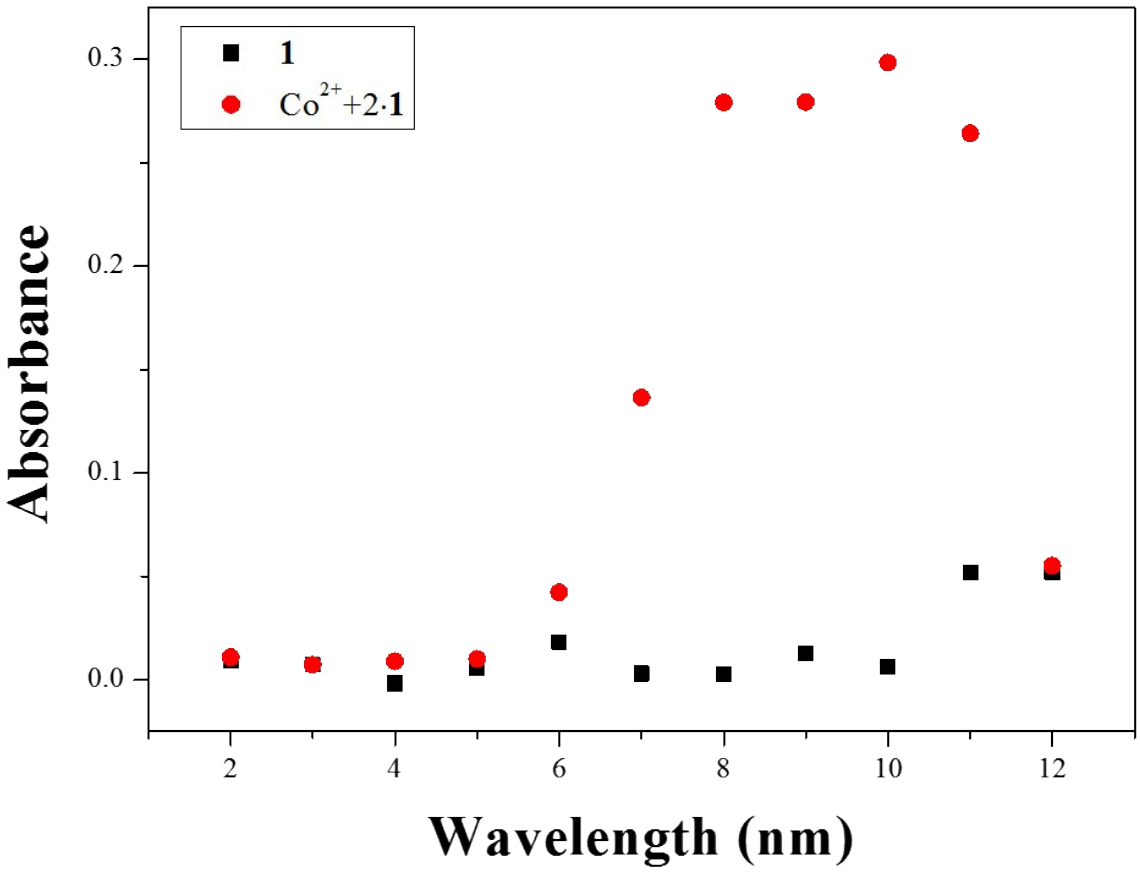

Fig. S4 UV-vis absorbance (400 nm) of **1** and Co^{2+}-2•**1** complex at different pH (2-12) in a mixture of bis-tris buffer/DMSO (95/5, v/v), respectively.

(a)

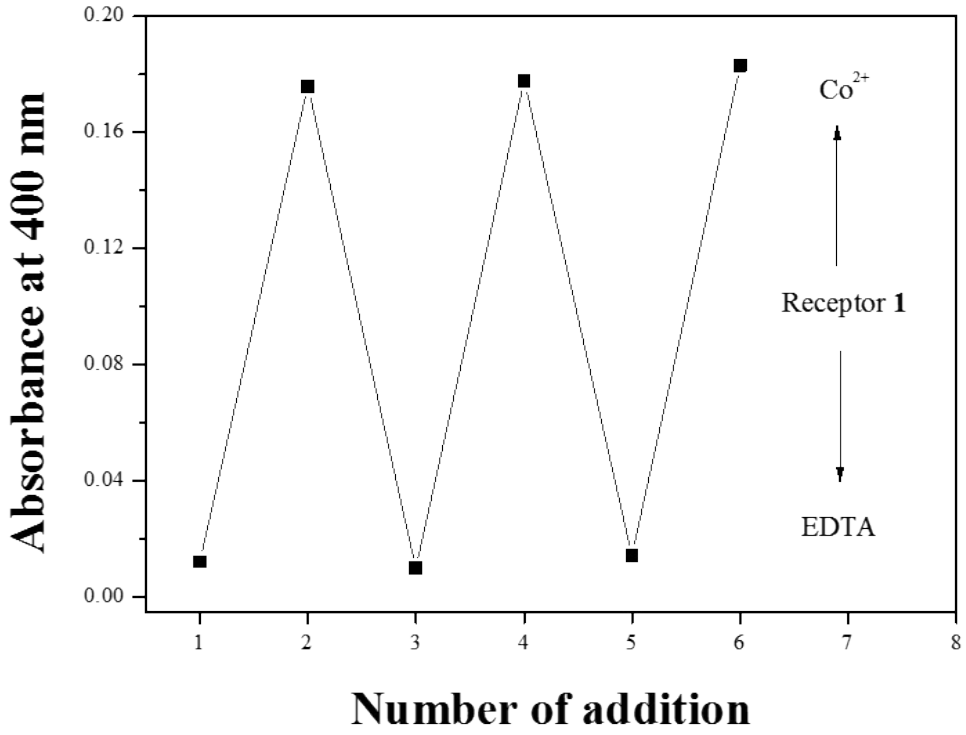

(b)

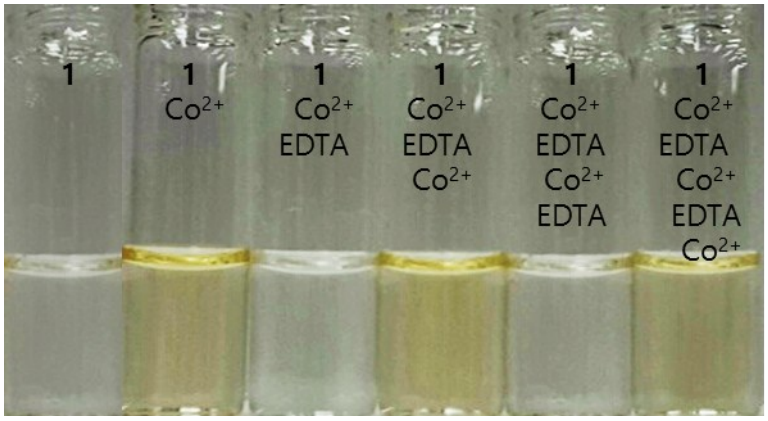

Fig. S5 (a) UV-vis spectral changes of **1** (20 μM) after the sequential addition of Co^{2+} and EDTA in bis-tris buffer/DMSO (95:5, v/v). (b) The color changes of **1** (20 μM) after the sequential addition of Co^{2+} and EDTA.

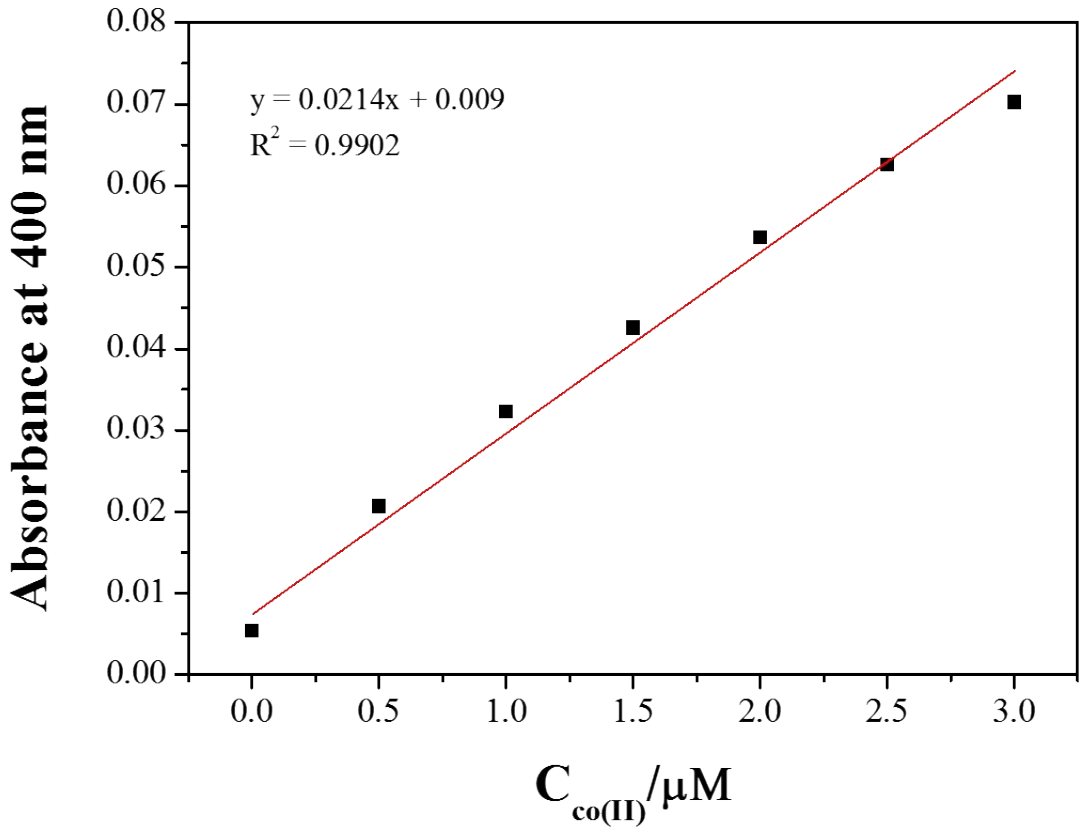

Fig. S6 Absorbance (at 400 nm) of **1** as a function of Co(II) concentration. [**1**] = 20 μmol/L and [Cu(II)] = 0.00-3.00 μmol/L in a mixture of bis-tris buffer/DMSO (95/5, v/v, 10 mM bis-tris, pH 7.0).

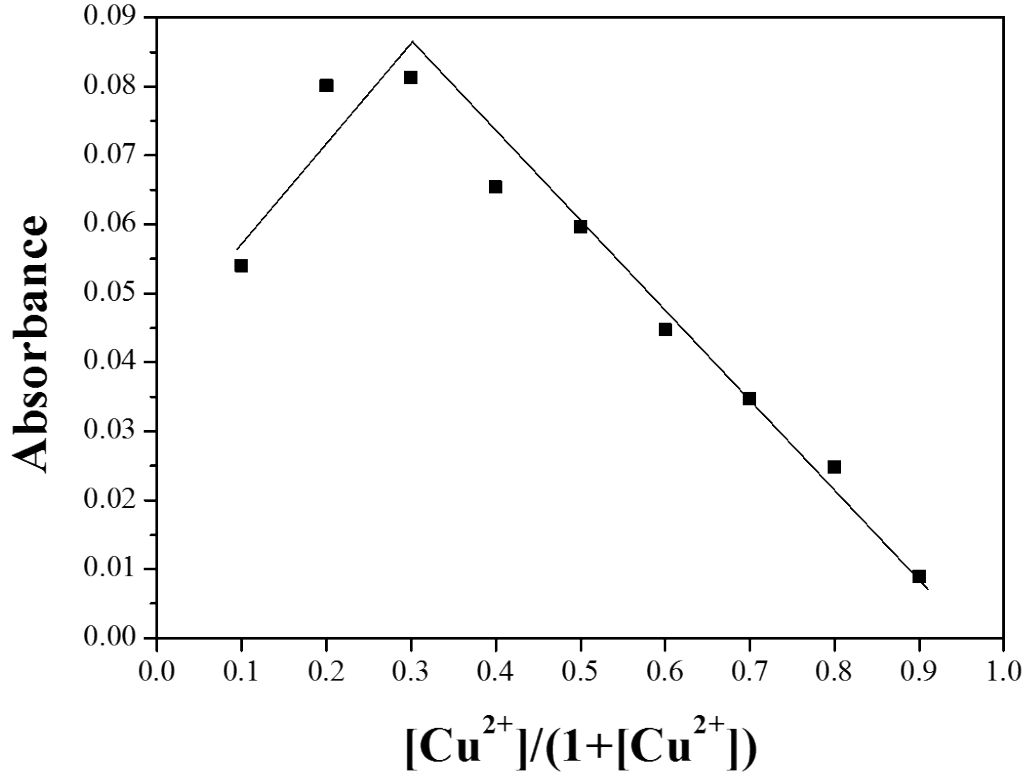

Fig. S7 Job plot for the binding of **1** with Cu^{2+}. Absorbance at 400 nm was plotted as a function of the molar ratio of $[Cu^{2+}]/([\mathbf{1}]+[Cu^{2+}])$. The total concentration of Cu^{2+} ions with receptor **1** was 2.0 x 10^{-5} M.

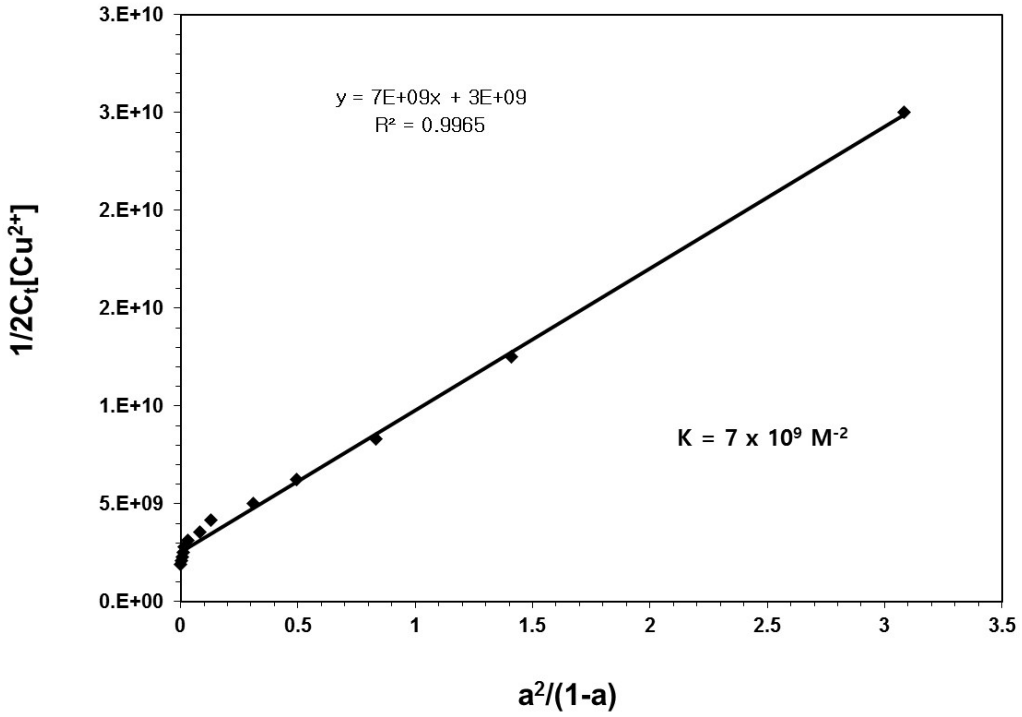

Fig. S8 Li's equation plot (absorbance at 400 nm) of **1**, assuming 2:1 stoichiometry for association between **1** and Cu^{2+}. 'Ct' means the concentration of **1**, and 'a' does $[(A_x-A_{max})/(A_0-A_{max})]$.

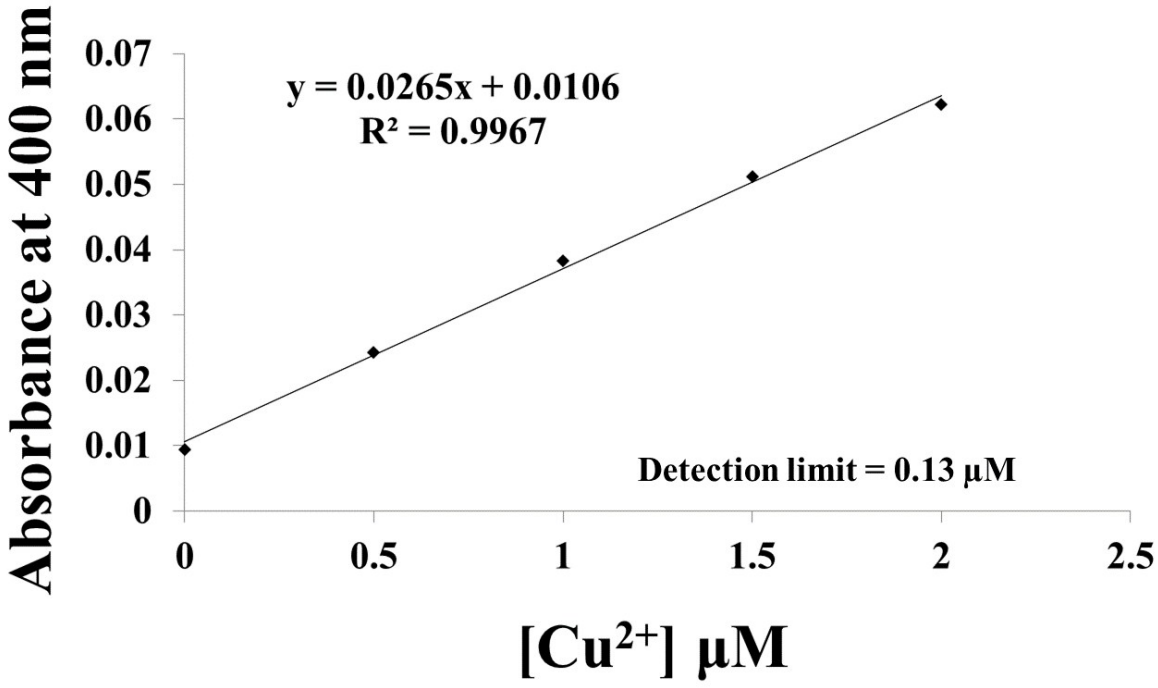

Fig. S9 Detection limit based on change in the ratio (absorbance at 400 nm) of **1** (20 μM) with Cu^{2+}.

(a)

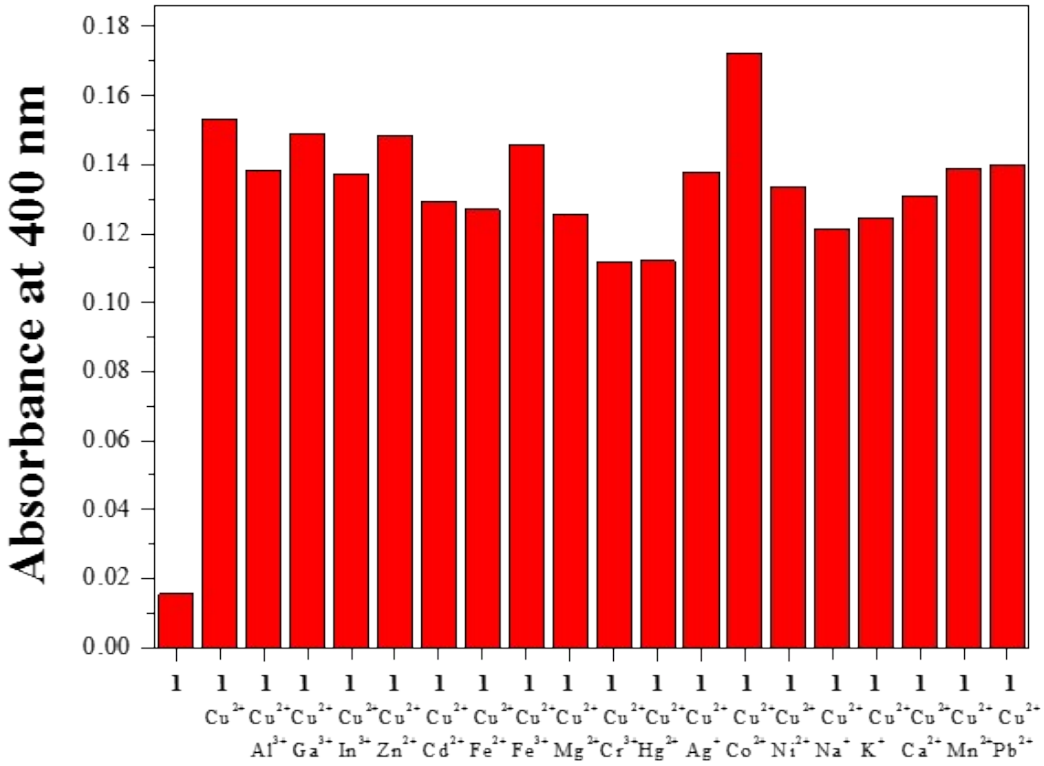

(b)

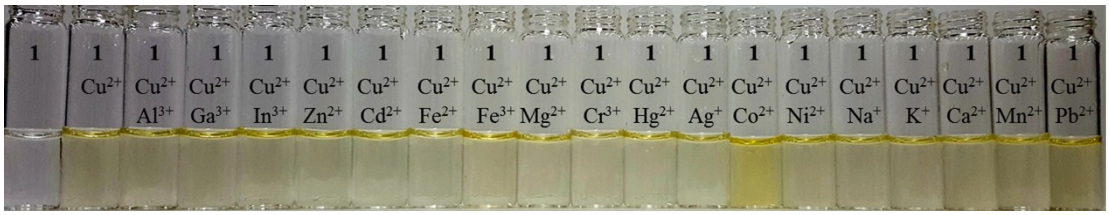

Fig. S10. (a) Absorption spectral changes of competitive selectivity of **1** (20 μM) toward Cu^{2+} (0.7 equiv) in the presence of other metal ions (0.7 equiv) in bis-tris buffer /DMSO (95/5, v/v). (b) The color changes of competitive selectivity of **1** (20 μM) toward Cu^{2+} (0.7 equiv) in the presence of other metal ions (0.7 equiv).

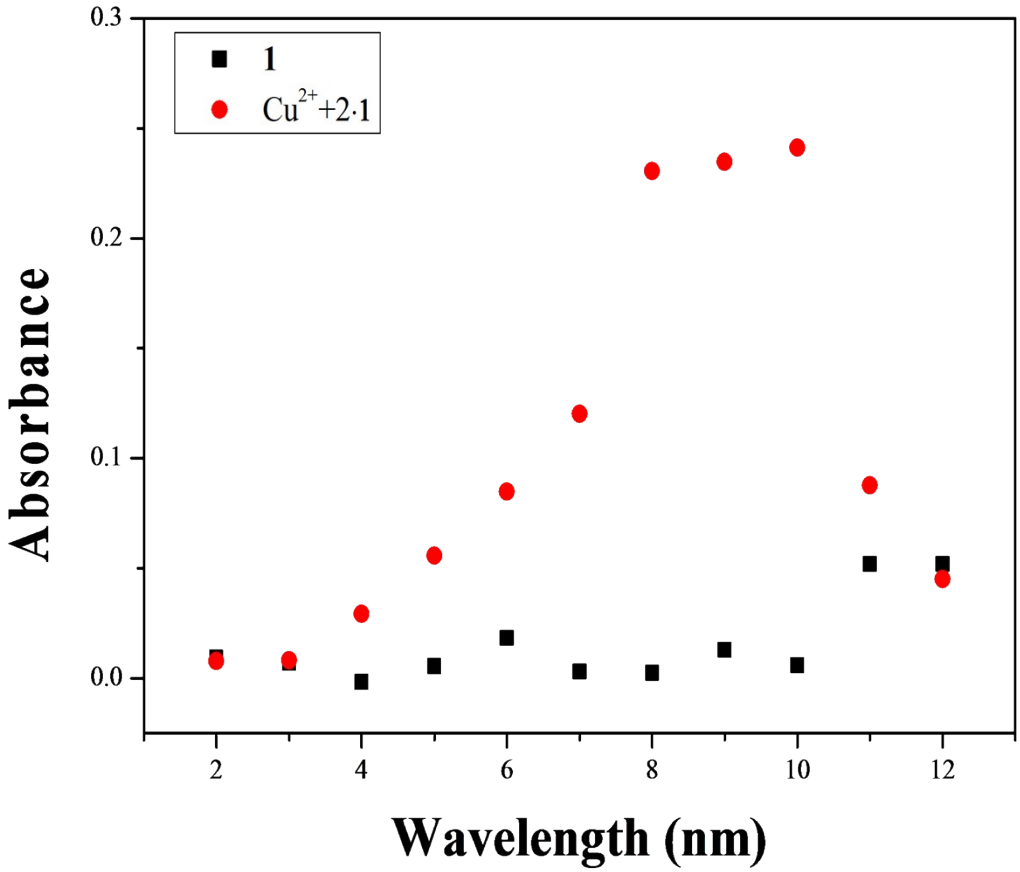

Fig. S11. UV-vis absorbance (400 nm) of **1** and Cu^{2+}-2•**1** complex at different pH (2-12) in a mixture of bis-tris buffer/DMSO (95/5, v/v), respectively.

(a)

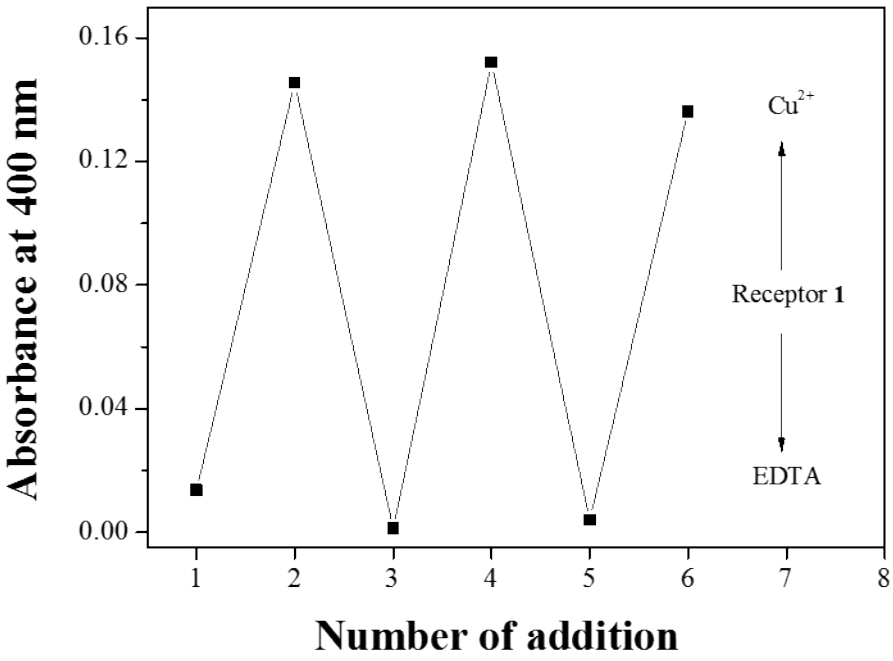

(b)

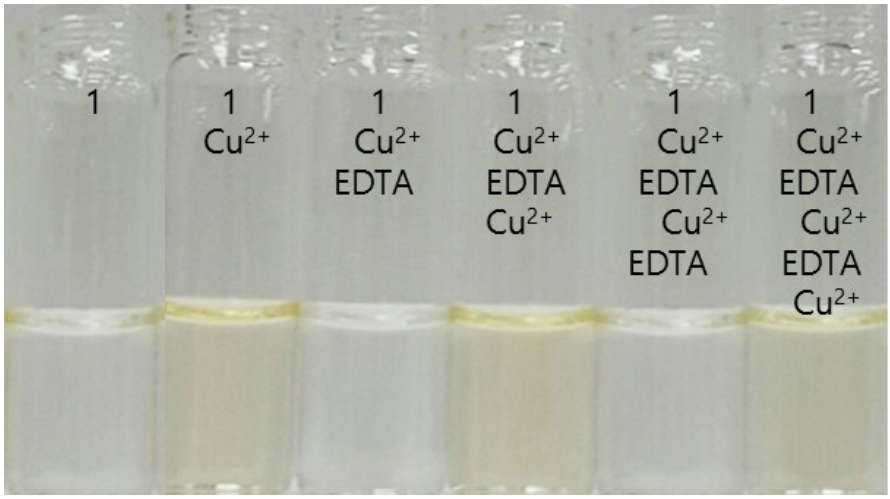

Fig. S12. (a) UV-vis spectral changes of **1** (20 μM) after the sequential addition of Cu^{2+} and EDTA in a mixture of bis-tris buffer/DMSO (95/5, v/v). (b) The color changes of **1** (20 μM) after the sequential addition of Cu^{2+} and EDTA.

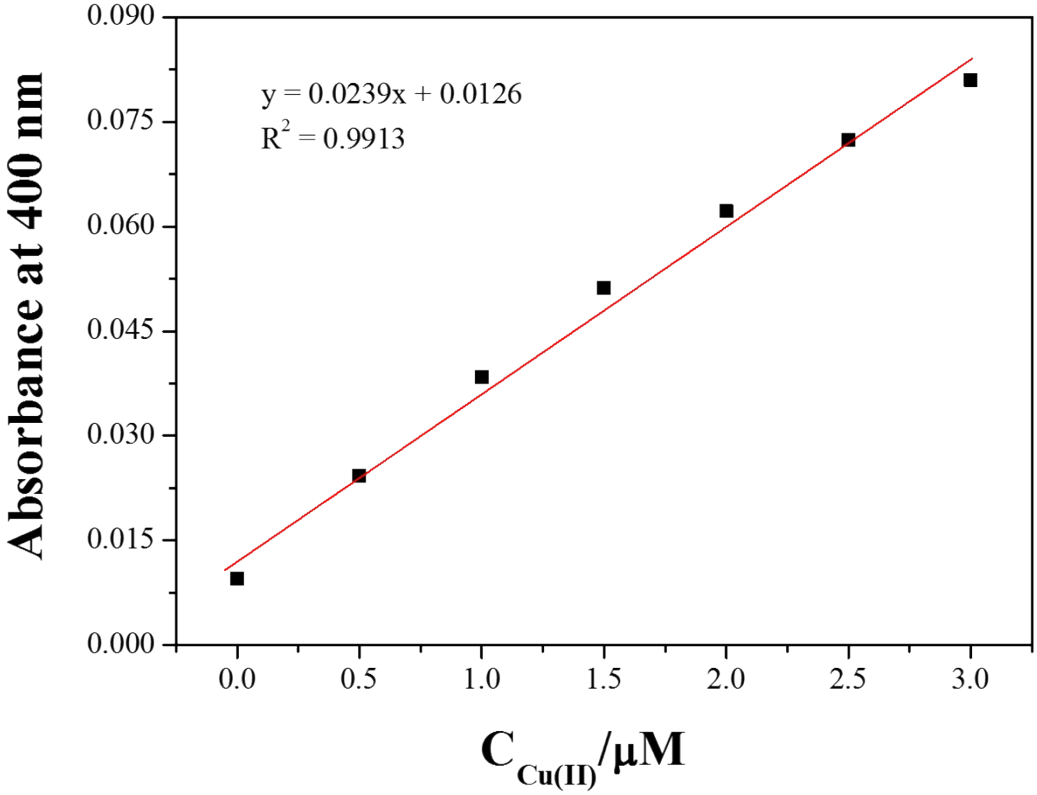

Fig. S13 Absorbance (at 400 nm) of **1** as a function of Cu(II) concentration. [**1**] = 20 μmol/L and [Cu(II)] = 0.00-3.00 μmol/L in a mixture of bis-tris buffer/DMSO (95/5, v/v, 10 mM bis-tris, pH 7.0).

(a)

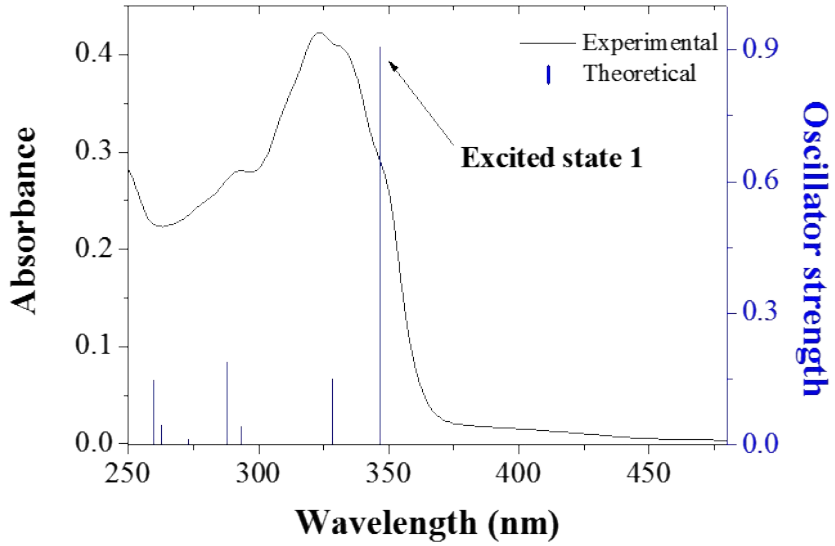

(b)

Excited State 1	Wavelength	Percent (%)	Character	Oscillator strength
H → L	346.8	98%	ICT	0.9049

(c)

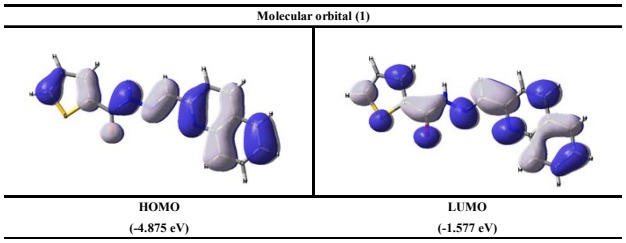

Fig. S14 (a) The theoretical excitation energies (TD-DFT method) and the experimental UV-vis spectrum of **1**. (b) The major electronic transition energy and molecular orbital contributions for **1** (H = HOMO and L = LUMO). (c) Isosurface (0.030 electron bohr-3) of molecular orbitals participating in the major singlet excited state of **1**.

(a)

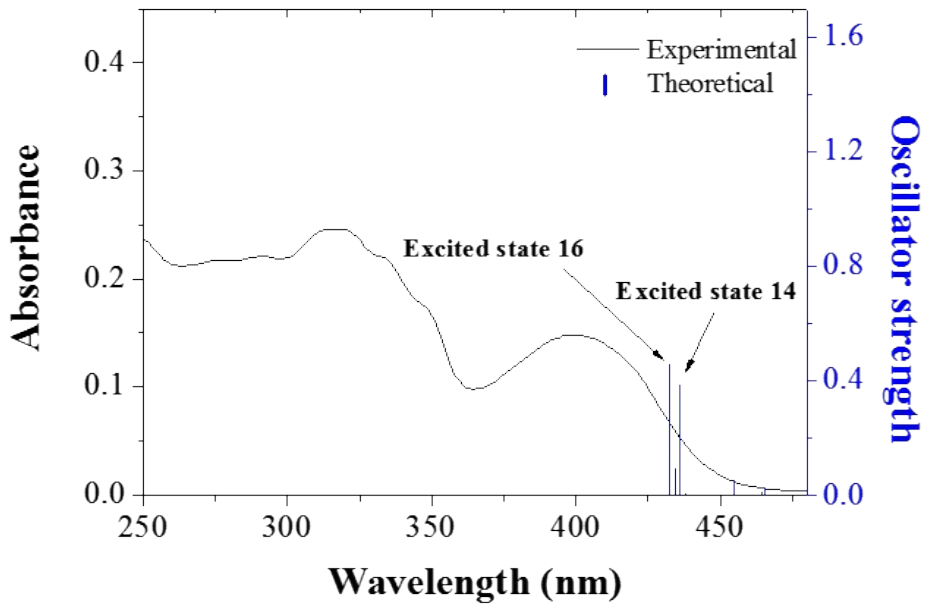

(b)

Excited State 14	Wavelength	percent (%)	Character	Oscillator strength
H-1 (α) → L (α)	435.75	18%	ICT	0.3857
H (α) → L+1 (α)		11%	ICT	
H-3 (β) → L (β)		19%	LMCT	
H-1 (β) → L+1 (β)		23%	ICT	

Excited State 16	Wavelength	percent (%)	Character	Oscillator strength
H-1 (α) → L+1 (α)	432.57	22%	ICT	0.4597
H-4 (β) → L (β)		22%	LMCT	
H-1 (β) → L+2 (β)		21%	ICT	
H (β) → L+1 (β)		10%	ICT	

(c)

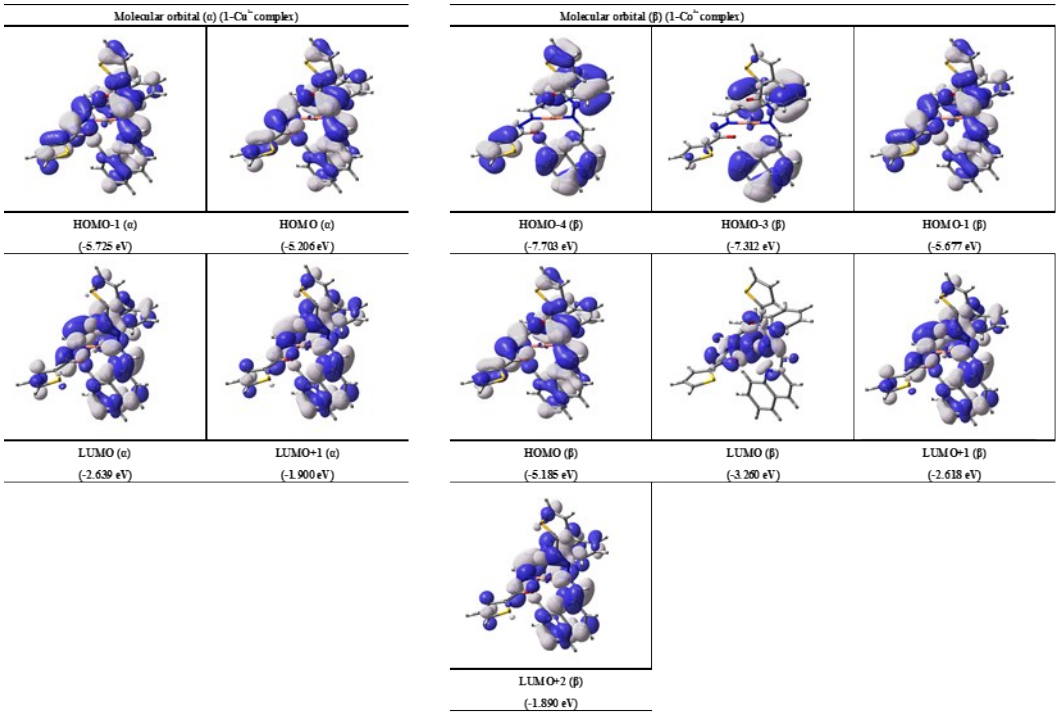

Fig. S15 (a) The theoretical excitation energies (TD-DFT method) and the experimental UV-vis spectrum of Cu^{2+}-2·**1** complex. (b) The major electronic transition energies and molecular orbital contributions for **1** (H = HOMO and L = LUMO). (c) Isosurface (0.030 electron bohr-3) of molecular orbitals participating in the major singlet excited state of Cu^{2+}-2·**1** complex.

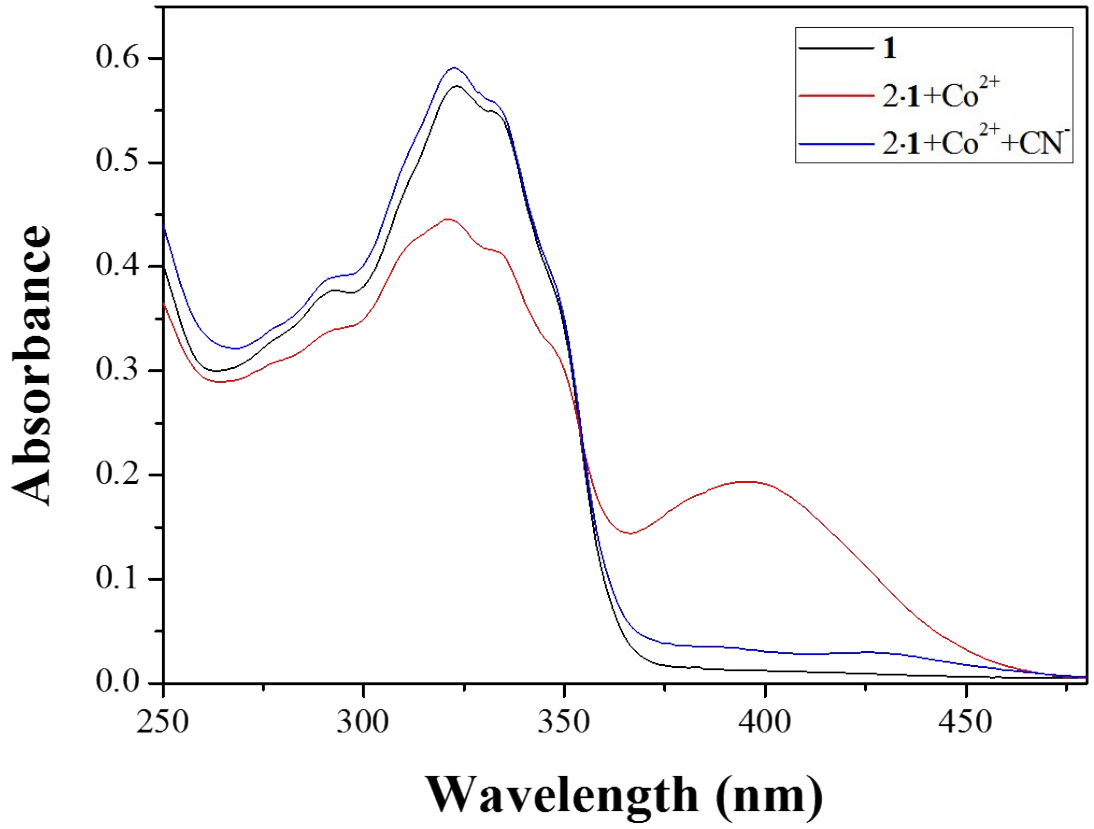

Fig. S16 UV-vis spectra of **1** (20 μM), Co^{2+}-2·**1** (Co^{2+} = 15 μM), and Co^{2+}-2·**1** + CN^- (30 equiv) in bis-tris buffer/DMSO (95/5, v/v).

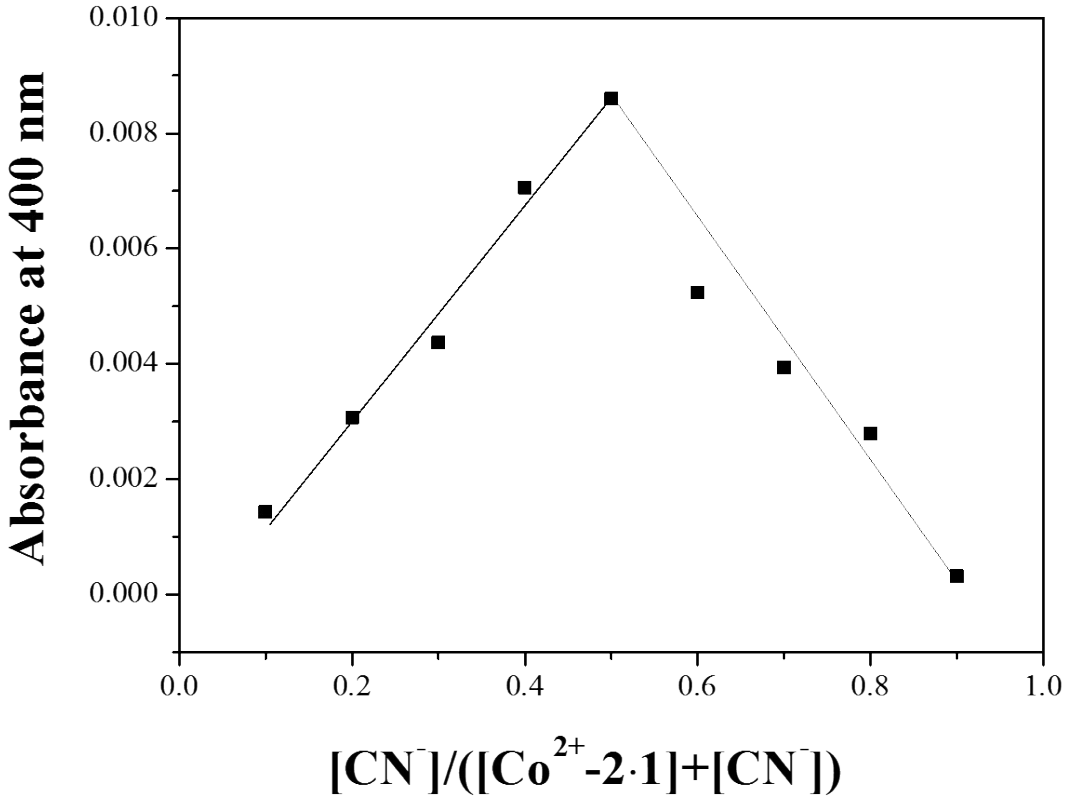

Fig. S17 Job plot of Co^{2+}-2·**1** complex and CN^-, where the intensity at 400 nm was plotted against the mole fraction of CN^-. The total concentrations of CN^- with Co^{2+}-2·**1** complex were 20 μM

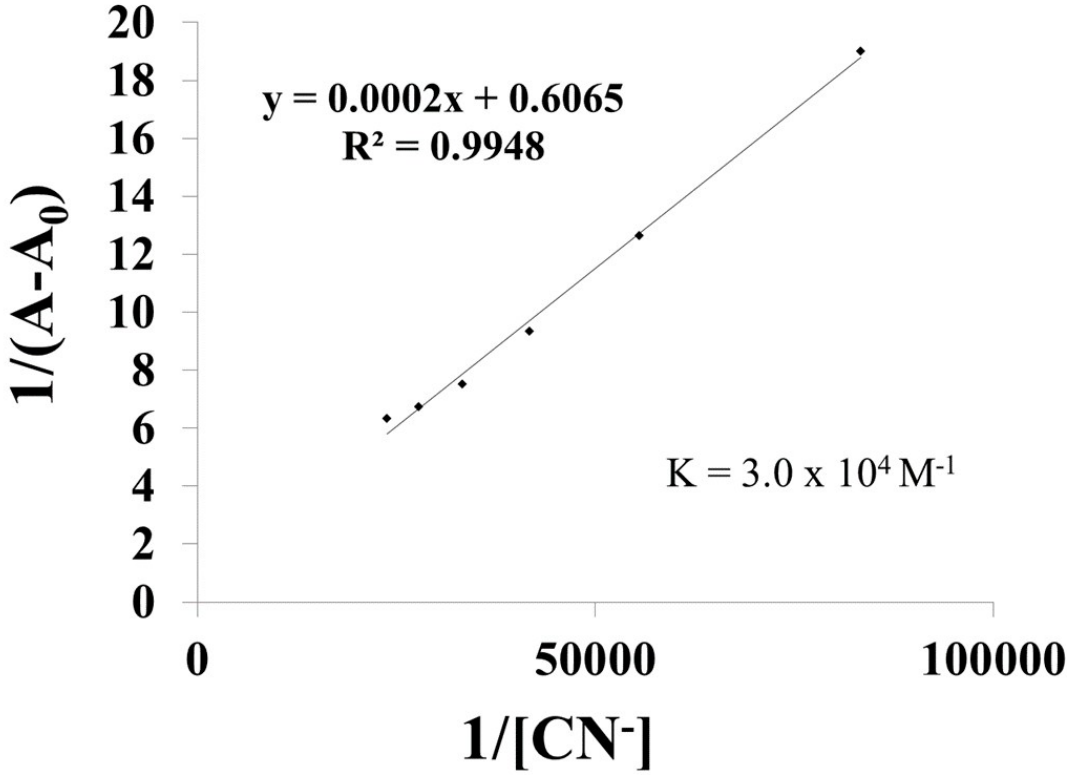

Fig. S18 Benesi-Hildebrand plot (at 400 nm) of Co^{2+}-2·**1** (20 μM), assuming 1:1 stoichiometry for association between Co^{2+}-2·**1** and CN^-.

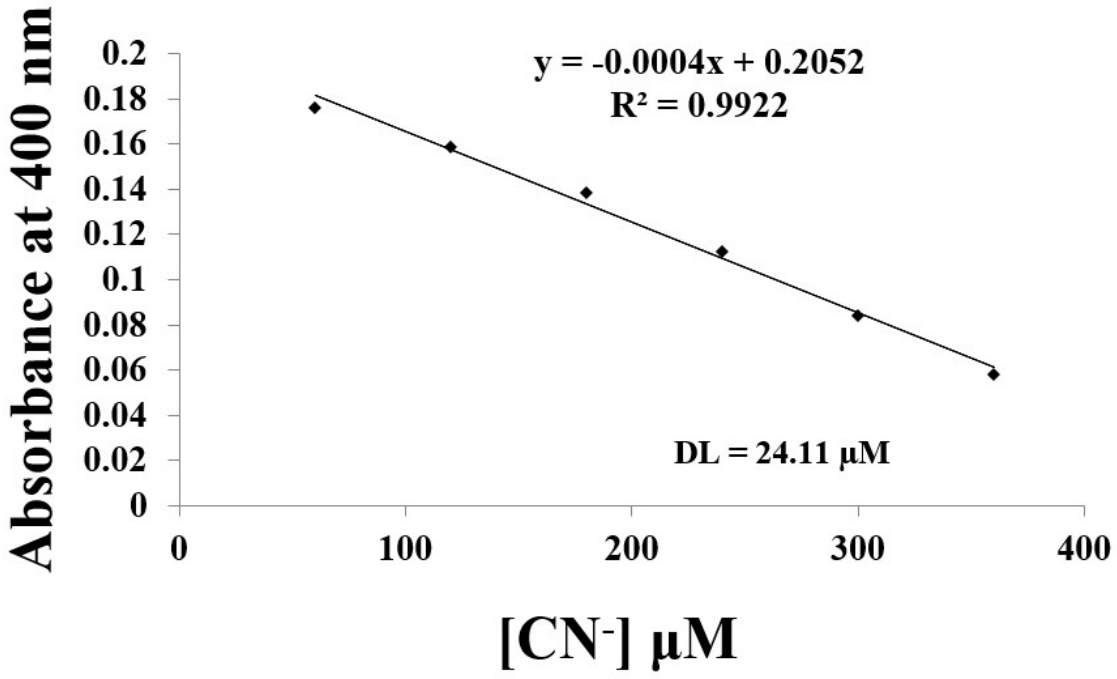

Fig. S19 Determination of the detection limit based on change in the ratio (absorbance at 400 nm) of Co^{2+}-2·**1** (20 μM) with CN^-.

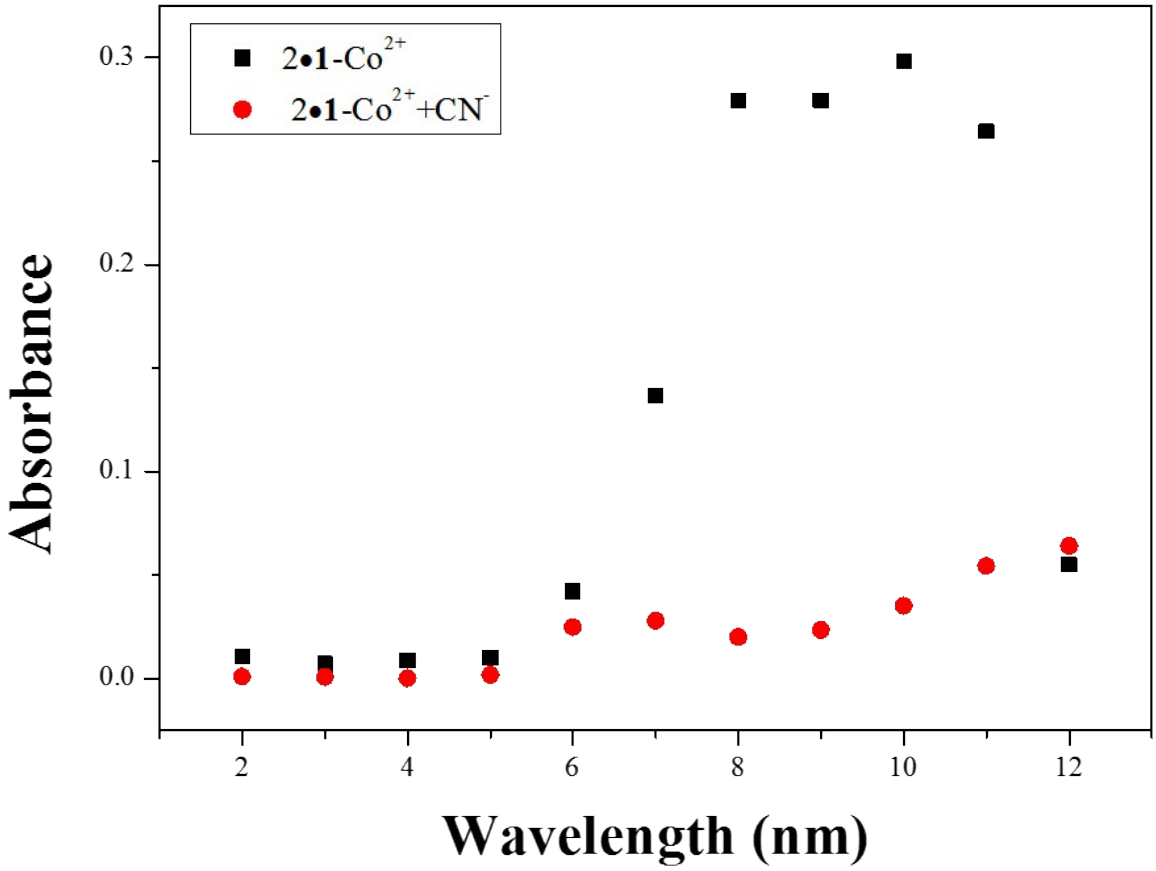

Fig. S20 UV absorbance (at 400 nm) of Co^{2+}-2·**1** (20 μM) and Co^{2+}-2·**1**-CN^- at different pH (2-12) in a mixture of bis-tris buffer /DMSO (95/5, v/v), respectively.